JOURNAL OF Applied Polymer SCIENCE

Preparation and Characterization of Melt-Blended Graphene Nanosheets-Poly(vinylidene fluoride) Nanocomposites with Enhanced Properties

M. El Achaby,[1,2] F. Z. Arrakhiz,[1,2] S. Vaudreuil,[1] E. M. Essassi,[1,2,3] A. Qaiss,[1] M. Bousmina[3]

[1]Moroccan Foundation for Advanced Science, Innovation and Research (MAsCIR), Institute of Nanomaterials and Nanotechnologies (NANOTECH), Rabat, Morocco

[2]Faculty of Science, Mohammed V-Agdal University, B.P. 1014 RP, Rabat, Morocco

[3]Hassan II Academy of Science and Technology, Rabat, Morocco

Correspondence to: A. Qaiss (E-mail: a.qaiss@mascir.com)

ABSTRACT: Nanocomposites of poly(vinylidene fluoride) (PVDF) with chemically reduced graphene nanosheets (GNs) were prepared by melt mixing method and their structure and morphology characterized by SEM analysis. The addition of GNs in the PVDF matrix resulted in changes of the crystallization and melting behaviors. Furthermore, increasing GNs content led to improved thermal stability of the PVDF nanocomposites in air and nitrogen, as well as significant increase in tensile and flexural properties. The nanocomposites' rheological behavior is also affected by the GNs' content. Using oscillatory rheology to monitor the GNs' dispersion, it was found that as the GNs loading increase, the Newtonian behavior disappears at low frequency. This suggests a viscoelastic behavior transition from liquid-like to solid-like, with greater GNs content and more homogeneous dispersion resulting in a stronger solid-like and nonterminal behavior. By using the melt mixing method to disperse GNs, the properties of PVDF are enhanced due to the better dispersion and distribution of GNs throughout the matrix. This improvement could broaden the applications for PVDF nanocomposites. © 2012 Wiley Periodicals, Inc. J. Appl. Polym. Sci. 000: 000–000, 2012

KEYWORDS: graphene, polymer nanocomposite; melt blending; thermal properties; mechanical properties

Received 15 December 2011; accepted 17 May 2012; published online
DOI: 10.1002/app.38081

INTRODUCTION

Since its discovery in 2004 by Geim and coworkers,[1] graphene has become an attractive material because of its superior electrical, thermal, and mechanical properties.[2–7] Graphene nanosheets (GNs) can be obtained directly in large quantities from graphite using low cost processes.[8–17] In the three-step graphene oxide route, natural graphite is first oxidized into graphite oxide (GO) using strong acids and oxidizing agents. Simple sonication in water yields a stable colloidal solution[13] after which chemical[11–17] or thermal reduction[10] is performed to yield GNs. Because of the structure defects generated during thermal reduction, chemical reduction is preferred to achieve the large scale graphene production ideally suited for polymer nanocomposite applications, with good thermal stability, large aspect ratio and high specific area.[18,19] This allows the use of conventional processing techniques to achieve low cost manufacturing of graphene-based polymer nanocomposites.

Two things must be achieved to carry over the exceptional properties of graphene in a polymer matrix. The first is the good dispersion and distribution of nanosheets in the polymer matrix while the second is a high degree of interaction between GNs and macromolecular polymer chains. Because GNs have strong tendency to agglomerate or to re-arrange into graphite structure due to strong van der Waals interactions, it is very difficult to re-exfoliate onto individual nanosheets during blending with a polymer. Different ways have been successfully developed to overcome these difficulties. Solvent mixing, melt mixing, and *in situ* polymerization are widely used techniques to produce graphene-based nanocomposites. To evaluate the quality of dispersion/distribution of GNs in these nanocomposites, different characterization techniques can be used including microscopy observations, X-ray diffraction (XRD) and rheology studies.[19–24]

While it have been demonstrated that solution-phase processing is the most common way to manufacture high performance graphene-based polymer nanocomposites at very low graphene content,[18–20] economic and environmental limitations make this method less desirable.[23]

Compared with solution blending, the use of melt mixing with commercial polymers and classical compounding systems such as twin screw extruder is very attractive as it provides many degrees of freedom with regard to the selection of polymer grades and choice of graphene loading.[25] Using a twin screw extruder, Kim et al. developed new strategies to polymer nanocomposites by incorporating of thermally reduced graphene (TRG) into a variety of polymer matrices such as poly(ethylene naphthalate) (PEN),[26] polycarbonate (PC),[27] polyurethane (PU),[23] and polyethylene (PE).[24] From their results, the electrical, mechanical, rheological and barrier to gases properties of these elastomers and engineering plastics can be significantly improved by incorporating less than 3 wt % of TRG. An electrically conductive polyethylene terephthalate (PET)-TRG nanocomposite was developed by Zhang et al. using melt mixing method,[25] with a low electrical percolation threshold of 0.47 vol %. Melt-extruded of TRG or exfoliated GO based polymer nanocomposites have been obtained from various polymers matrices such as polypropylene (PP), styrene acrylonitrile (SAN), and polyamide (PA-6).[28]

Poly(vinylidene fluoride) (PVDF) is a semicrystalline polymer with remarkable properties such as a thermal stability, inflammability, excellent chemical resistance, and high mechanical strength combined with very low creep. The use of graphene derivatives, at very low content, to reinforce PVDF properties could broaden the applications for PVDF nanocomposites. Ansari et al. prepared PVDF nanocomposites with TRG or expanded graphite (EG) from solution mixing method. The mechanical, thermal and electrical properties of such FGS-based PVDF nanocomposites were characterized and a percolation threshold was observed at around 2 wt %, a value lower than the 5 wt % found in EG-filled PVDF composites.[29] Layek et al. recently used PMMA-modified GNs to reinforce PVDF using solvent mixing. Because the successfully functionalization of graphene sheets resulted in an improved compatibility with PVDF, superior properties were achieved.[30] High performance nanocomposite materials have also been reported by incorporating the graphene oxide nanosheets into PVDF matrix via solution mixing approach.[31]

In a previous work, we incorporated chemically reduced GNs into polyolefin matrix using melt extrusion.[32] Results from this work have shown that the GNs were successfully dispersed into the polymer matrix, yielding improved thermal, mechanical and rheological properties at low GNs content. We report here the preparation of PVDF nanocomposites with chemically reduced GNs via melt compounding approach. The thermal, tensile, flexural and rheological properties of the resulting nanocomposites were characterized. Improvement in properties could lead to new applications for PVDF.

MATERIALS AND EXPERIMENTAL METHODS

Materials

Natural powder graphite (<20 μm; 99.99%), concentrated sulfuric acid (H_2SO_4; 99%), hydrochloric acid (HCl; 5%), sodium nitrate ($NaNO_3$; ≥99.0%), potassium permanganate ($KMnO_4$; 99%), hydrogen peroxide (H_2O_2; 30%) and hydrazine hydrate ($N_2H_4{\cdot}H_2O$; 80%) were purchased from Sigma-Aldrich. A commercial grade of polyvinylidene fluoride (PVDF; Kynar 1000HD, density of 1.77 g/cm^3) was obtained from Arkema. All materials were used as received.

GNs Preparation

GO was prepared via chemical oxidation of natural graphite according to Hummers' method.[33] In this procedure, H_2SO_4, $NaNO_3$, and $KMnO_4$ are used to oxidize the graphite after which dilution and washing are performed with distilled water. Residual metallic ions are removed by the use of hydrogen peroxide and hydrochloric acid. The GO are then isolated through centrifugation and drying. To exfoliate GO into individual graphene oxide sheets, the desired amount of GO is dispersed in water and then sonicated for 1 h, resulting in yellow-brownish colloidal solution.[32] GNs are obtained by the reduction of graphene oxide with hydrazine hydrate as reducing agent. This reaction is performed at a temperature of 95°C for 1 h, using an ammonium solution to adjust pH at a value of 10. Subsequent filtration, washing and drying yield a large amount of chemically reduced graphene oxide nanosheets, referred as GNs. The overall steps for GNs preparation are given in Figure 1(a).

Preparation of GNs-Filled PVDF Nanocomposites

PVDF nanocomposites containing various GNs contents (from 0.5 to 4 wt %) were prepared by melt-compounding in a laboratory scale twin-screw mixer (Haake Minilab II). Compounding was performed at 230°C for s using a screw speed of 100 rpm. Before compounding, PVDF was grinded in a fine powder (FRITSCH Pulverisette 19 equipped with a 0.2-mm sieve size) and dried overnight at 60°C. All samples for characterizations and measurements were prepared by hot-press molding at a temperature of 230°C, including neat PVDF for comparison. The overall steps for nanocomposites preparation are shown in Figure 1(b).

Characterization Techniques

Wide-angle XRD characterizations of graphite derivatives were carried out on Bruker D8 Discover using the CuKα radiation (λ = 1.54184 nm). Fourier transform infrared spectroscopy (FTIR) was performed using an ABB FTLA2000 equipped with a Specac Golden gate single reflection ATR accessory. Tapping mode atomic force microscopy (AFM) measurements were carried out on a Veeco Dimension Icon. The sample used for AFM imaging was prepared by placing a drop of dispersed graphene solution onto a freshly cleaved mica surface. Thermal stability was evaluated by thermogravimetric analyses (TGA) using a Q500 TGA system from TA Instrument. Analyses of graphite derivatives were carried out under air at a heating rate of 5°C min^{-1} from 25 to 700°C, while analyses of nanocomposite samples were carried out under nitrogen and air at a heating rate of 10°C min^{-1}. A lower heating rate was used only for graphite derivatives to approximate the thermal exposure encountered during melt mixing and so evaluate their possible thermal degradation. Differential scanning calorimetry (DSC) measurements of nanocomposites were carried out under nitrogen gas using a DSC Q100 (TA Instrument) in the −70 to 230°C range. To remove the samples' thermal history, an initial heating phase to 230°C for 5 min was done after which they were cooled down to −70°C before initiating the actual test. Cooling and heating

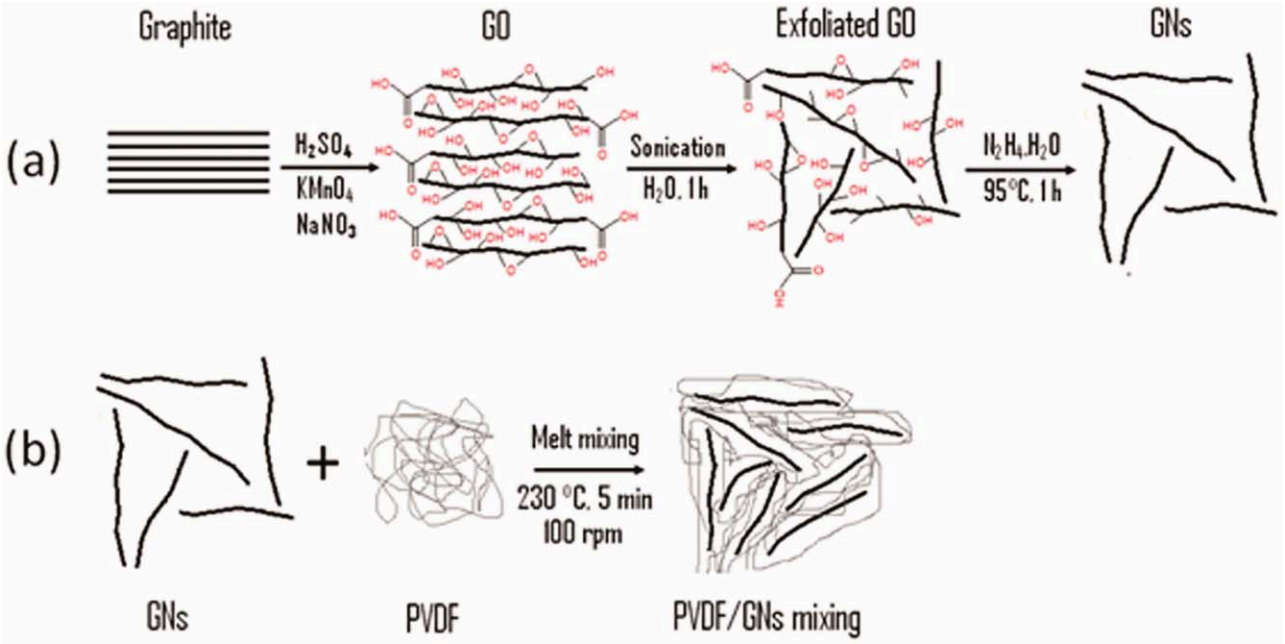

Figure 1. Schema of overall steps of (a) GNs preparation and (b) GNs-filled PVDF preparation. [Color figure can be viewed in the online issue, which is available at wileyonlinelibrary.com.]

were performed at the same rate of 10°C/min. Cooling and heating were performed at the same rate of 10°C/min. Sample morphology was characterized by scanning electron microscopy (SEM) using a JEOL JSM-5500 operating at 16 kV. Tensile and flexural tests were performed using an Instron 8821S tensiometer according to procedures ISO 527-2 and ASTM D790-03, respectively. For tensile tests, dog bone-shaped specimens with a gauge length of 25 mm, a width of 5 mm and a thickness of 2 mm were prepared by hot-compression at 230°C. All tensile tests were performed at 25°C and with a stretching speed of 5 mm/min, without any preconditioning on the samples. Young's modulus was calculated from the linear region of the stress–strain data (from strain values between 0.005 and 0.025 mm/mm). Bending tests were conducted using a three-point bending configuration at a crosshead motion rate of 2.55 mm/min and support span set at 49.5 mm. Rectangular specimens with a length of 70 mm, width of 10 mm and thickness of 1.6 mm were used. Dynamic rheology measurements were performed on a strain-controlled rotational rheometer (ARES-LS, Rheometrics Instruments). Measurements were carried out at 230°C in oscillatory shear mode using parallel plate geometry (25 mm in diameter). The 1-mm thick sample disks were molded in the same conditions as those for tensile test samples. Strain sweeps were applied at a frequency of 0.1 Hz while frequency sweeps ranging from 100 to 0.01 Hz were performed at 2% strain. In these conditions, the materials exhibit a linear viscoelastic behavior. Specimens were allowed to equilibrate for ~ 5 min prior to each sweep run.

RESULTS AND DISCUSSION

GNs Characterization

Production of GNs from graphite by the graphene oxide route was confirmed through the use of XRD, AFM, FTIR, and TGA measurements. XRD show that the reflection peak at $2\theta = 26.23°$ ($d = 0.34$ nm) in graphite shifts to $2\theta = 10.4°$ ($d = 0.85$ nm) in GO (Figure 2). In addition, the absence of secondary peaks is a sign of a complete oxidation of graphite into GO. The complete exfoliation and chemical reduction of GO into graphene was also confirmed by XRD as no secondary or characteristic peaks have been observed (Figure 2), thus confirming the removal of all periodic structures.

AFM in tapping mode is used to evaluate both thickness and morphology of the as-prepared GNs. Figure 3 shows a representative AFM image of GNs deposited on cleaved mica surface. The cross-sectional view reveals an average thickness for the graphene sheets of ~1 nm which is similar to values obtained by other groups.[7,18,34] The slightly higher thickness when

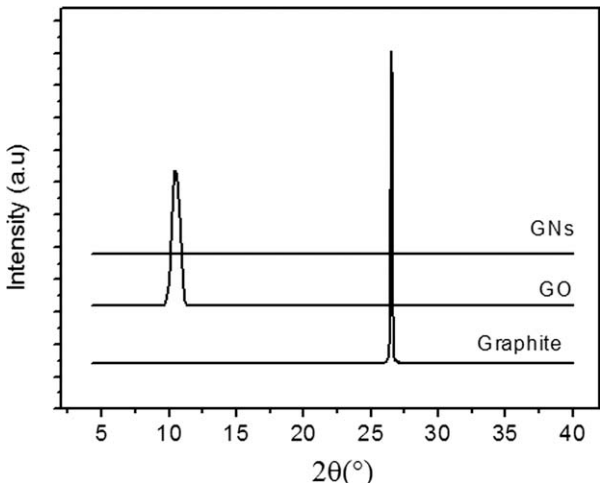

Figure 2. XRD patterns of pristine graphite, GO, and GNs.

Applied Polymer SCIENCE

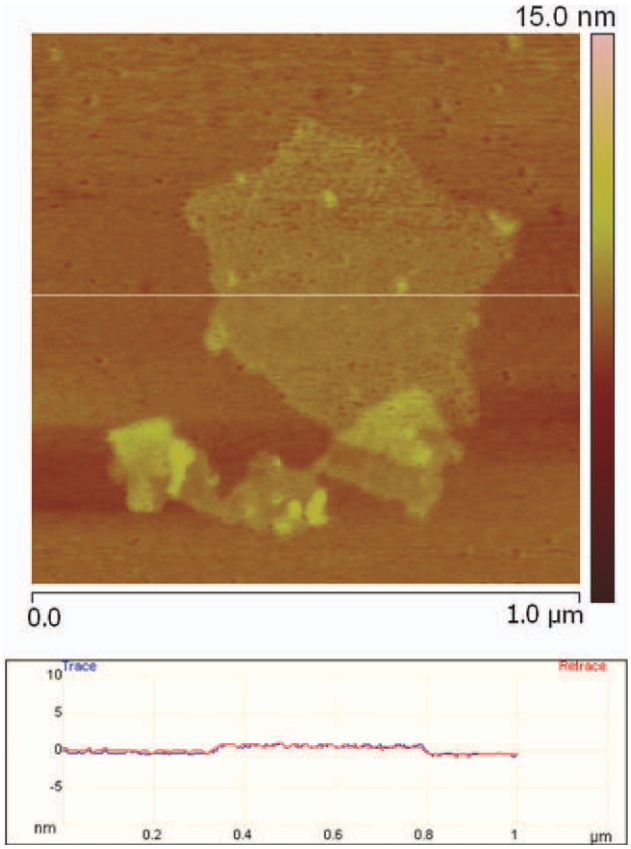

Figure 3. Tapping mode AFM image of exfoliated GNs and its corresponding height profile (under image) along the indicated straight line. [Color figure can be viewed in the online issue, which is available at wileyonlinelibrary.com.]

compared against the ~ 0.8 nm measured by other groups[16,19] can be explained by the wrinkling of graphene during solvent evaporation. Consequently, AFM confirmed the production of single layer graphene because the measured thickness of 1 nm is half than the thickness of bilayer graphene (~ 2 nm).[10]

FTIR analyses of graphene oxide revealed the formation of carboxyl, epoxide and peroxide functional groups during the chemical oxidation of graphite, as well as water molecules (Figure 4). However, the bands at 3680 cm^{-1} and 1410–1280 cm^{-1} can be attributed respectively to the stretching and in-plane deformation of the O—H bonds in hydroxyl groups. The intense peaks between 1600 and 1800 cm^{-1} can be assigned to the stretching vibration of C=O in carboxyl groups while the bands at 1000 and 1150 cm^{-1} are assigned to C > O in epoxide. Several C—H bands can also be found between 2000 and 3340 cm^{-1}. The peak at 3800 cm^{-1} is been attributed to H_2O molecules and indicates that GO was intercalated to some extent by water.[35,36] The FTIR spectrum of GNs is devoid of noticeable absorption bands, indicating that H_2O molecules and most of the oxygen-containing groups were totally removed during the chemical reduction of GO (Figure 4). Those results are in good agreement with previous literature work, confirming the reduction of GO in graphene.[25,36,37]

The thermal stability of GO and GNs in air was studied by TGA and the results were compared with that of pristine graphite (Figure 5). Graphite starts to lose weight progressively at 650°C by combustion, leading to the formation of carbon dioxide.[14] In the case of the thermally unstable GO, it decomposes following a three steps process beginning with the loss of residual water in the initial stage of heating. The second step corresponds to the decomposition of the most labile oxygen functionalities present in the material which begins at around 200°C. The slow and steady mass loss observed in the whole temperature range above 350°C can be ascribed to degradation of more stable oxygen functional groups.[38] The last step is attributed to the carbon oxidation occurring between 450 and 650°C.[13,14] The reduced graphene oxide (GNs) shows a relatively strong thermal stability in regard to unreduced GO. The loss of mass at around 200°C is very small, indicating the efficient removal of oxygen functional groups after reduction.[13,14,16] However, in agreement with previous reports[13,14,16,38] the observed mass loss for the reduced GNs in the temperature range above 350°C, suggesting that the reduction processes cannot remove the most stable functionalities. Total decomposition of GNs occurs through carbon oxidation between 450 and 675°C, something which was previously reported in literature.[14] It can be observed that such oxidation mechanism for GNs occurs at a lower temperature than that of pristine graphite

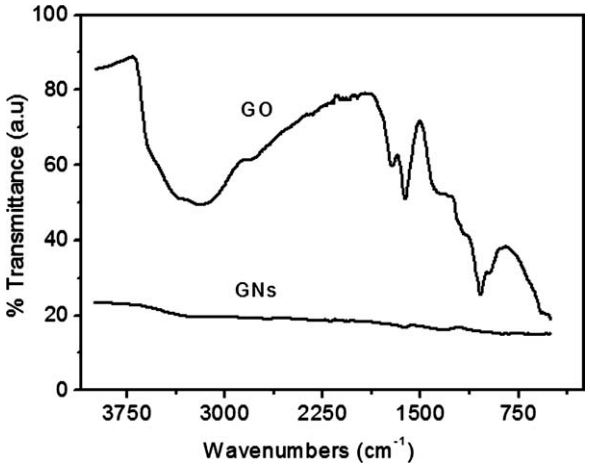

Figure 4. FTIR spectra of GO and GNs.

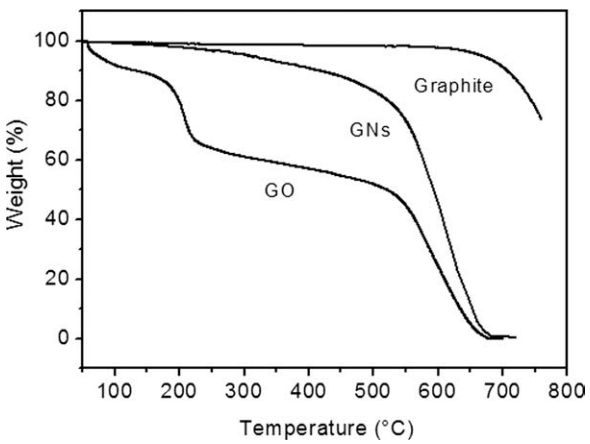

Figure 5. TGA curves of pristine graphite, GO, and GNs.

(450°C instead of 650°C). Removal of the layered structure in exfoliated GNs and the presence of defects generated during the oxidation/reduction process can explain such significant decrease in temperature.

PVDF Nanocomposite Characterizations

SEM Characterizations. To determine the quality of the GNs dispersion in PVDF, SEM was employed. Figure 6 shows the SEM images of fracture surfaces of neat PVDF and GNs-filled PVDF nanocomposites containing 1.5 and 3 wt % GNs. It can be seen that the fractured surface of neat PVDF polymer is rather flat and smooth [Figure 6(a)]. In contrast, the images of nanocomposite materials show that most of GNs are fully exfoliated and clearly well dispersed, while there are a few restacks together [Figure 6(b, c)]. In addition, it is clear that the GNs are randomly dispersed within the matrix, which is an important phenomenon for improvement of mechanical properties of fabricated nanocomposites. Consequently, the melt mixing technique was appropriate to obtain a homogeneous distribution of nanosheets within the PVDF polymer.

Crystallization and Melting Properties

The crystallization and melting properties of neat PVDF and its GNs nanocomposites were studied as function of GNs content. It is to be noted that mechanical properties of semicrystalline polymer are related to the internal microstructure and crystallinity.[39] DSC crystallization [Figure 7(a)] and melting [Figure 7(b)] curves from first cooling and second heating cycles for neat PVDF and its GNs nanocomposites have been used to evaluate the thermal parameters. Table I resumes the crystallization ($T_{c\ \mathrm{onset}}$ and $T_{c\ \mathrm{peak}}$) and melting ($T_{m\ \mathrm{onset}}$ and $T_{m\ \mathrm{peak}}$) temperatures, as well as the crystallization enthalpy (ΔH_c), heat of fusion (ΔH_m) and percentage of crystallinity (X_c) as function of GNs content. The relative X_c was calculated from the melting enthalpy using the following expression: $X_c = (\Delta H_m/(1 - x)\Delta H_0) \times 100$, where ΔH_m is the heat of fusion of samples, ΔH_0 is the theoretical heat of fusion value for a 100% crystalline PVDF and is equal to 104.6 J/g,[40] and x is the weight fraction of GNs in the each sample.

Addition of GNs affects the crystallization temperatures of neat PVDF by resulting in an increase with larger GNs content. While the crystallization peak temperature, $T_{c\ \mathrm{peak}}$, of neat PVDF was found at around 147.7°C, it increased to 153.3°C in nanocomposites with 3 wt % GNs. The same upward trend was observed in the onset crystallization temperature ($T_{c\ \mathrm{onset}}$). This indicates that GNs plays a dominant role in accelerating crystallization of PVDF when cooled from the melt, because of a heterogeneous nucleation effect in the nanocomposite materials.

GNs addition has no substantial effects on the melting temperatures $T_{m\ \mathrm{onset}}$ and $T_{m\ \mathrm{peak}}$ which are respectively of $\sim$ 142°C and $\sim$ 170°C for both neat PVDF and PVDF nanocomposites. The melting enthalpy (ΔH_m) of neat PVDF is also not significantly affected by addition of GNs (Table I).

The degree of crystallinity (X_c) of neat PVDF and its nanocomposites was calculated from the melting enthalpy (ΔH_m) and results show that no significant change were observed with the presence of GNs (Table I).

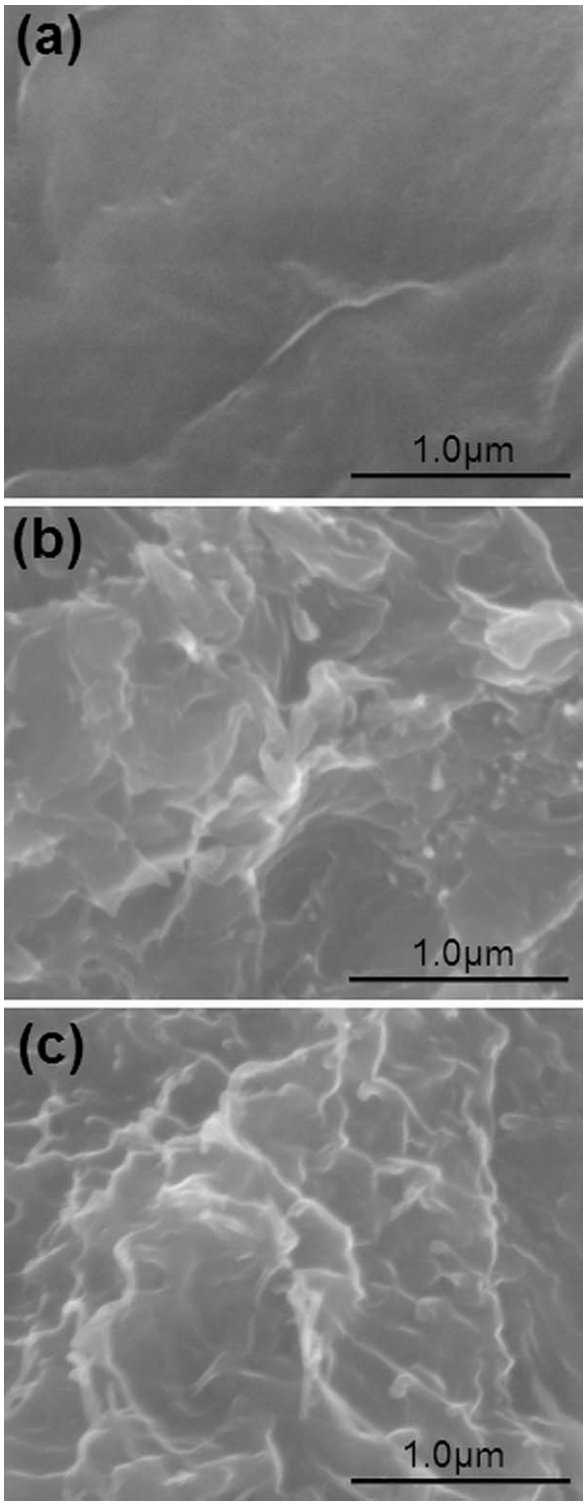

Figure 6. SEM images of the fracture surface of (a) neat PVDF and its nanocomposites containing (b) 1.5 wt % and (c) 3 wt %.

Thermal Stability

The thermal stability of graphene-based polymer nanocomposites is of interest because of the good thermal stability of GNs at the processing temperature used for most elastomers and engineering plastics.[41] It has been reported that graphene can

Applied Polymer SCIENCE

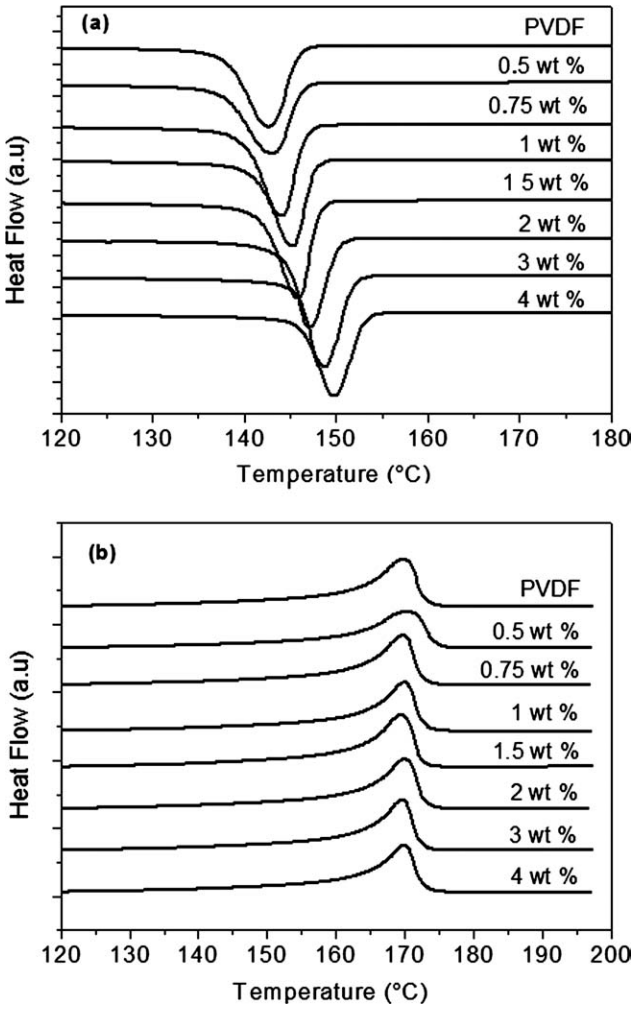

Figure 7. Crystallization (a) and melting (b) thermograms of PVDF and its nanocomposites at indicated weight fraction of GNs.

increase the thermal stability of polymers such as PMMA,[20] PS,[41] and PVDF.[30] Some of the key factors affecting thermal stability of graphene-filled polymer nanocomposites are the structure of the matrix and the level of interfacial interaction between graphene sheets and polymer chains.

Thermal degradation of extruded GNs-based PVDF nanocomposites was evaluation in both air and nitrogen environments, with TGA and DTG curves found in Figure 8. Results show that PVDF nanocomposites exhibit a noticeable increase in thermal stability with increasing GNs content, especially at the onset of degradation. For neat PVDF and GNs-filled PVDF nanocomposites, a single-step decomposition process is observed under nitrogen environment as shown in Figure 8(a, b). The situation is different for GNs-based PVDF nanocomposites under air as decomposition occurs in a three-step process which ends by the carbon oxidation at 550°C of GNs as CO_2. In the case of neat PVDF, complete decomposition in air occurs in two steps below 550°C [Figure 8(c, d)].

Analysis of the TGA data was done on the basis of temperature at a weight loss at 5% ($T_{5\%}$) and the temperature at maximum decomposition rate (T_{max}) to understand the effect of GNs addition, the data of $T_{5\%}$ and T_{max} are shown in Table II. Results show that the thermal stability of neat PVDF and its nanocomposites is higher in nitrogen than in air where the presence of oxygen favors rapid thermo-oxidation degradation.[42] Neat PVDF begins to decompose in air and nitrogen respectively at a temperature of $\sim$ 390°C and $\sim$ 420°C, with $T_{5\%}$ being 27°C higher in nitrogen than in air. This trend was observed in all PVDF nanocomposites where values in nitrogen are being higher than those in air.

Thermal stability of nanocomposites was found to increase with increasing GNs content but not in a linear manner, regardless of atmosphere. The addition of just 0.5 wt % of GNs increased $T_{5\%}$ temperature in GNs/PVDF nanocomposite by 18°C in nitrogen, but an eight-time increase in GNs (to 4%) only yielded an increase of 36°C (Table II). In air, the addition of 0.5 wt % of GNs result in an increase of 20°C in $T_{5\%}$ with a maximum increase of 52°C when 4 wt % of GNs are added. These results show that the benefits on thermal stability of adding GNs in a PVDF matrix are more noticeable in air than in nitrogen, even at low GNs loading.

The maximum temperature of decomposition (T_{max}) in GNs-filled PVDF nanocomposites also shows increase with increasing GNs loading in both air and nitrogen (Table II). In nitrogen, T_{max} for the single step decomposition process goes from 463°C

Table I. Onset Temperature of Crystallization (T_{conset}), Peak Temperature of Crystallization (T_{cpeak}), Crystallization Enthalpy (ΔH_c), Onset Temperature of Melting (T_{monset}), Peak Temperature of Melting (T_{mpeak}), Heat of Fusion (ΔH_m) and Degree of Crystallinity (X_c) for PVDF and its Nanocomposites at Indicated Weight Fraction of GNs

GNs content	T_{conset} (°C)	T_{cpeak} (°C)	ΔH_c (J/g)	T_{monset} (°C)	T_{mpeak} (°C)	ΔH_m (J/g)	X_c (%)
PVDF	147.7	142.6	45.9	141.2	169.7	46.3	44.3
0.5 wt %	147.9	143.0	43.8	141.9	170.3	43.1	41.3
0.75 wt %	148.3	144.0	45.3	143.8	169.6	45.0	43.3
1 wt %	149.3	145.1	42.4	140.9	169.8	45.1	43.6
1.5 wt %	149.6	145.7	46.5	141.4	169.4	48.7	47.3
2 wt %	151.7	147.1	41.6	144.5	169.8	44.8	43.7
3 wt %	153.3	148.7	42.7	141.7	169.6	45.1	44.5
4 wt %	154.5	149.7	41.5	141.1	169.8	43.3	43.2

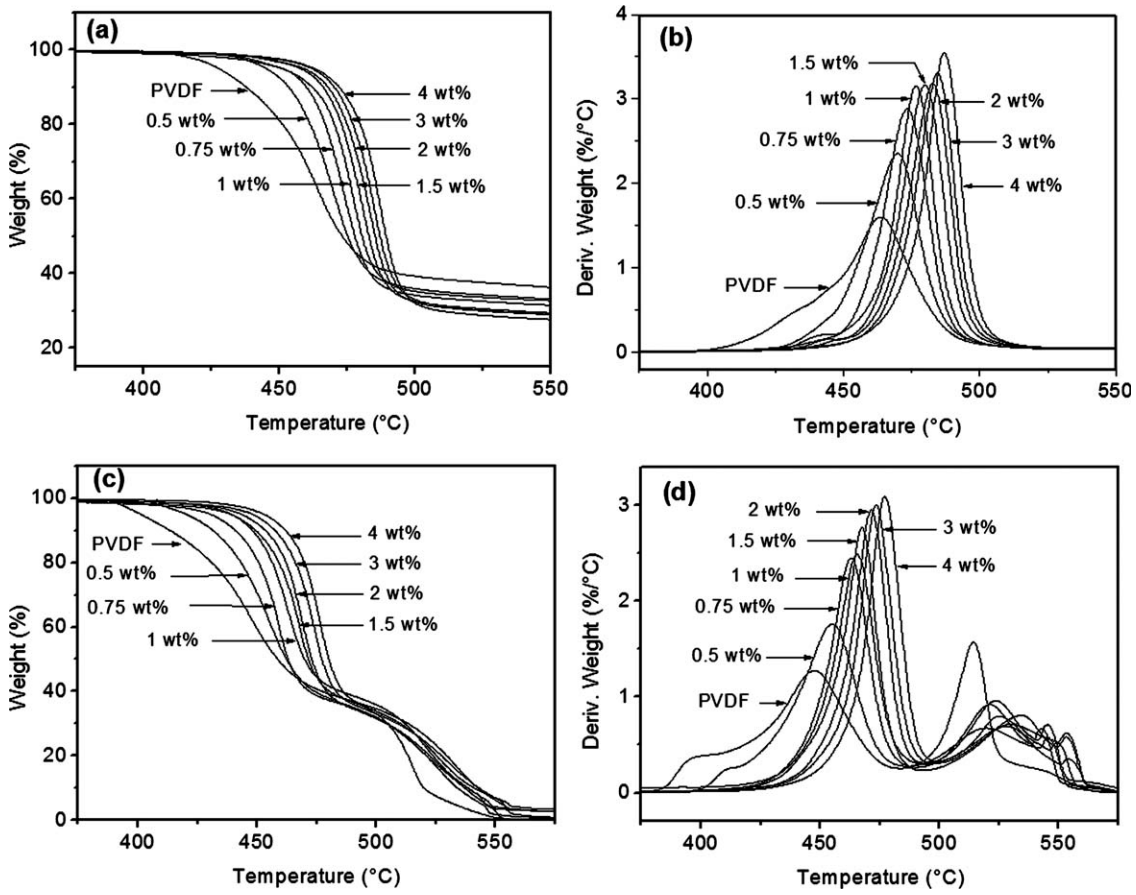

Figure 8. Thermal stability of PVDF and its nanocomposites at indicated weight fraction of GNs, with (a) TGA and (b) DTG curves carried out under nitrogen and (c) TGA and (d) DTG curves carried out under air.

for neat PVDF to 487°C when 4 wt % of GNs is added. In the case of air, the two-step decomposition process of PVDF is affected differently. While the increase of GNs content results in an increasingly higher T_{max1} value, the T_{max2} show some increase at first before dropping significantly after exceeding a critical GNs content of ~ 2 wt % (Table II). From a maximum of ~ 534°C at 2 wt % GNs loading, the T_{max2} value is only 434°C at 3 wt % GNs.

The stabilization observed with the addition of GNs can be attributed to a barrier effect by homogenously dispersed nanosheets which limit the diffusion of oxygen from the gas phase into the bulk nanocomposite and the decomposition products from the bulk polymer onto the gas phase.[43,44] The presence of significant interfacial interactions between nanosheets and polymer matrix also lead to an increase in the activation energy of degradation, resulting in an improvement in thermal degradation resistance.

Dynamic Rheological Properties

Fabrication of graphene-based polymer nanocomposites by melt mixing remains a challenge due to graphene's high aspect ratio and specific surface area that results in strong individual interactions and possible poor dispersion in the matrix. So to characterize the dispersion quality of GNs fillers, percolated rheological network structure and relative interaction between polymer chains and fillers, the dynamic rheological properties of neat PVDF and GNs-reinforced PVDF nanocomposites were measured through oscillatory shear.

To help select the strain appropriate for the linear viscoelastic behaviors of these nanocomposites, dynamic strain sweeps were

Table II. Temperature Corresponding to a Weight Loss of 5% (T5%) from TGA Analyses Under Nitrogen and Air, Maximum Decomposition Temperatures Under Nitrogen (T_{max}) and Under Air (T_{max1} and T_{max2}) from DTG Analyses for PVDF and its Nanocomposites at Indicated Weight Fraction of GNs

	Under nitrogen		Under air		
GNs content	$T_{5\%}$ (°C)	T_{max} (°C)	$T_{5\%}$ (°C)	T_{max1} (°C)	T_{max2} (°C)
PVDF	427.5	463.3	400.7	447.5	514.3
0.5 wt %	445.1	469.1	420.3	455.3	519.5
0.75 wt %	450.8	473.3	430.6	463.3	521.3
1 wt %	451.3	476.1	438.8	465.5	523.6
1.5 wt %	457.7	479.6	439.0	467.1	534.7
2 wt %	458.3	482.2	443.4	471.1	534.7
3 wt %	461.1	484.1	447.6	473.5	433.3
4 wt %	463.3	487.4	452.8	477.4	434.2

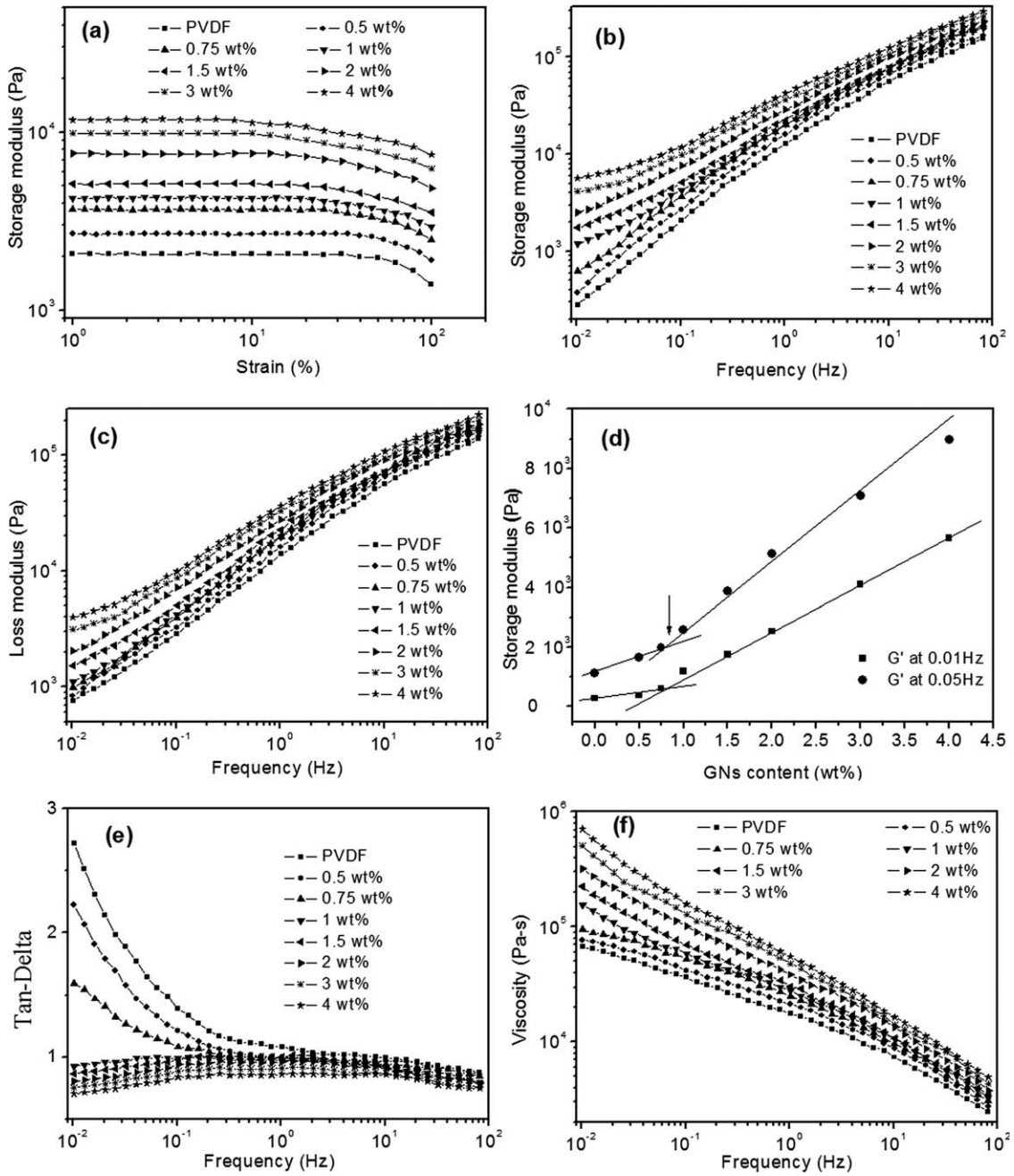

Figure 9. Dynamic rheological properties of PVDF and its nanocomposites at indicated weight fraction of GNs, with (a) storage modulus versus strain, (b) storage modulus versus frequency, (c) loss modulus versus frequency, (d) storage modulus versus GNs content, (e) tan δ versus frequency, and (f) complex viscosity versus frequency.

first collected for all samples at 0.1 Hz and 230°C. Figure 9(a) shows the strain (γ) dependence of dynamic storage modulus (G') for nanocomposite systems with different GNs loading. For neat PVDF, the G' starts to drop drastically when strain exceed 30%, indicating the destruction of the material structure. In GNs-filled PVDF nanocomposites, G' increase monotonously with increased GNs loading due to a reinforcement effect by GNs. Nanocomposites containing 0.5 and 0.75 wt % GNs show the same trend that of neat PVDF in terms of critical strain limit (γ_{crit}) in the linear region. In PVDF nanocomposites containing $\geq$1 wt % GNs, however, the critical strain decreased more dramatically with increasing of GNs loading. A critical strain of 8.5% was observed for the nanocomposite with 4 wt % GNs, indicating that the structure of nanocomposites with high GNs loading levels start to destroy rapidly in comparison with that of neat polymer or nanocomposites with little GNs (0.5 and 0.75 wt % loading). This behavior was also previously observed by Kim et al. in TRG oxide-reinforced polyethylene naphthalate (PEN).[26] To avoid structure breakdown, a strain of 2% was chosen as appropriate strain to study the linear

viscoelastic behaviors in all nanocomposite samples. Dynamic frequency sweeps with an applied strain level of 2% were collected at 230°C for all samples. Storage modulus (G'), loss modulus (G''), tan (δ), and complex viscosity (η^*) were measured as a function of frequency in the linear viscoelastic region.

Results have shown that the storage modulus of GNs-filled PVDF nanocomposites increase with increasing GNs content through the full frequency range [Figure 9(b)]. At low-frequencies, PVDF chains are fully relaxed and display typical homopolymer-like terminal behavior. Addition of up to 0.75 wt % in GNs increased the storage modulus without changing the viscoelastic behavior, indicating that there is no enough GNs content to restrain polymer chain relaxation. Only when GNs loading reach or exceed 1 wt % that the G' starts to develop a plateau at low frequency. This is indicative of a transition from liquid-like to solid-like viscoelastic behavior. This nonterminal behavior at low frequency can be attributed to the formation of an interconnected graphene network in the polymer matrix which restrains the long-range motion of polymer chains.[26] The threshold at 1 wt % GNs could be explained by the interactions between individual GNs, leading to percolation and formation of an interconnected network structure in the polymer. G'' exhibits a similar trend than G' at low frequency in which G'' increase with increasing GNs loading [Figure 9(c)]. The increase in G'' is lower than what is measured in G' for the same GNs content however.

Figure 9(d) illustrates the variation of G' as function of GNs content for 0.01 and 0.05 Hz frequencies. We can see that G' increases rapidly when the GNs content exceed 0.75 wt %, indicating that the rheological percolation threshold is around 1 wt % GNs content. The formation of solid-like percolated network of GNs nanosheets can also be deduced from comparison between G' and G'' at a fixed GNs content. Figure 9(e) shows the variation of tan δ (G''/G') as function of frequency. At a low frequency, neat PVDF and nanocomposites with low GNs content ($\leq$0.75 wt %) exhibit a dominant viscous behavior. Only when GNs loading is $\geq$1 wt % that the elastic behavior becomes dominant.

Figure 9(f) shows the complex viscosity against frequency at various GNs contents. An increase in complex viscosity with increasing GNs content can be seen for the full frequency range. PVDF nanocomposites with 0.5 and 0.75 wt % GNs content exhibits the same behavior as neat PVDF, with weak increases in complex viscosity for the entire frequency range. For GNs content higher than 1 wt %, the viscosity rapidly increase, leaving only shear thinning in full frequency range (0.01–100 Hz). Furthermore, the sample roughly exhibits a linear relationship (log-log) throughout the studied frequency range, this being indicative of a yield stress. It has been widely shown that the existence of this transition is related to nanofiller-polymer interactions and the formation of a combined network of polymer chains and nanofiller.[26]

Mechanical Properties

The improvement of mechanical properties of nanocomposite polymers is related to the fillers' intrinsic mechanical properties, their homogeneity of dispersion and the extent of stress transfer between polymer chains and nanofillers. It has been reported that individual graphene sheets show extremely high values of fracture strength (125 GPa), Young's modulus (1000 GPa)[3] as well as a large aspect ratio and high surface area.[18,20] Because of this, the incorporation of exfoliated GNs into PVDF polymer should have a significant effect on the mechanical properties.

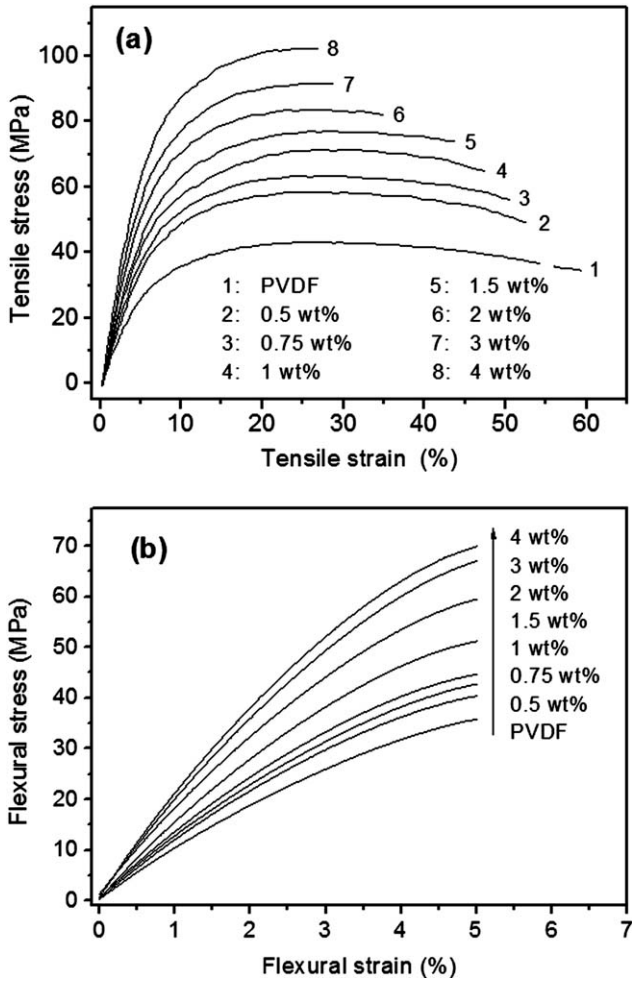

Figure 10. Typical stress–strain curves obtained from (a) tensile tests and (b) flexural tests of PVDF and its nanocomposites at indicated weight fraction of GNs.

Tensile properties of extruded neat PVDF and GNs nanocomposites were obtained from uniaxial tensile testing. From the stress–strain curves [Figure 10(a)], a significant increase of some tensile properties is achieved with the addition of GNs content. The Young's modulus (E) for example, increased from 1302 MPa (neat PVDF) to 3173 MPa (4 wt % GNs content) (Table III). The ultimate tensile strength (σ_s) also shows significant improvement, going from 43 MPa for neat PVDF to 102 MPa in nanocomposite with 4 wt % GNs. Only the elongation at break (ε_b) was reduced from 178% in neat PVDF to 27% in nanocomposites containing 4 wt % GNs, suggesting that the presence of GNs restricts the movement or mobility of polymer chains, as show by rheological measurements, thus leading to the brittleness of the nanocomposite materials.

The increase in modulus achieved by adding GNs is larger than what has been reported by various groups working on the melt-extrusion of TRG sheets-reinforced polymer.[26,27] Kim et al. studied

Table III. Mechanical Properties Obtained from Both Tensile and Flexural Tests for PVDF and its Nanocomposites at Indicated Weight Fraction of GNs

	Tensile properties			Flexural properties	
GNs content	Young modulus (MPa)	Tensile strength (MPa)	Elongation at break (%)	Flexural modulus (MPa)	Flexural stress at 5% (MPa)
PVDF	1302.4	43.1	178.4	1118.6	35.9
0.5 wt %	1624.4	58.6	87.2	1298.2	40.4
0.75 wt %	1712.7	63.4	62.5	1352.0	42.8
1 wt %	2051.3	70.9	55.5	1454.2	44.7
1.5 wt %	2190.7	77.2	43.8	1683.9	51.2
2 wt %	2583.1	83.7	35.0	1886.8	59.6
3 wt %	2812.4	91.8	28.9	2138.1	67.1
4 wt %	3173.6	102.5	26.9	2285.4	69.9

the effect of TRG on the elastic modulus of PEN and PC polymer prepared by melt-mixing approach. They observed a 25% increase in Young's modulus for PC nanocomposite with 2.5 wt %, and a 57% increase for PEN nanocomposite containing 4 wt % of TRG sheets.[26,27] Such increases can only be explained by the presence of specific interactions between the graphene filler and the polymer chains. Modified clay nanoparticles, which is a filler with comparable aspect ratio to graphene, did not yield significant improvement in tensile strength and Young's modulus when melt-extruded with PVDF at levels between 0.5 and 5 wt %.[45,46]

Three point flexural tests were used to evaluate the effect of GNs on the bending properties of PVDF polymer and GNs-reinforced PVDF nanocomposites. From load-deflection data, the flexural stress–strain curves were extracted according to ASTM D790-03 and presented in the Figure 10(b). Results show that the addition of GNs leads to an increase in bending properties, with the flexural modulus increasing from 1118 MPa for neat PVDF to 2285 MPa for 4 wt % GNs nanocomposite. The obtained data of flexural modulus are shown in Table III.

It should be noted that neither PVDF nor nanocomposites reached breaking point at a 5% strain because most plastics do not break from deflection. The flexural strength can be given in flexural stress when a 5% strain ($\sigma_{f5\%}$) occurs in thermoplastics and elastomers, strain which was extracted as a maximum point. However, the $\sigma_{f5\%}$ increased with addition of GNs, going from 35 MPa for neat PVDF to 70 MPa for nanocomposite with 4 wt % of GNs (Table III). While flexural modulus and flexural stress keep improving with increasing GNs content, the gains achieved when the GNs level exceed 3 wt % show the possible formation of agglomerates which can limit further increases in bending properties.

Such improvement in mechanical properties of prepared nanocomposites is due to the presence of strong interfacial interaction between PVDF chains and GNs and good dispersion homogeneity which are required to improve interfacial stress transfer from the polymer matrix to the individual GNs nanosheets, thus increasing nanocomposite stiffness and mechanical properties.

CONCLUSION

High performances graphene-filled PVDF nanocomposites were successfully prepared by incorporating chemically reduced GNs into PVDF matrix using small scale, twin-screw extruder. Morphology of these nanocomposites was investigated throughout SEM characterization and the results show a good homogeneity after melt blending. Rheology of the nanocomposites in the melt phase was performed to investigate the proper dispersion and distribution of GNs within the matrix. GNs-based PVDF nanocomposites show a linear viscoelastic behavior characterized by a reduction in critical strain, the formation of GNs networks in the polymer matrix and the transition from liquid-like to solid-like behavior, resulting in a dramatic increase in complex viscosity and storage modulus. DSC study shows that GNs acts as nucleating agents during PVDF crystallization and results in a gradual increase in crystallization temperature (T_c) with increasing of GNs content. This does not affect the melting properties however. The thermal and thermo-oxidative stability of nanocomposites were largely improved by addition of GNs, more noticeably in air. The high intrinsic mechanical properties of graphene and the relatively strong interaction between nanosheets and polymer, as well as the homogeneity of dispersion/distribution of nanosheets into PVDF, have significantly enhanced the mechanical properties. Young's modulus, flexural modulus, tensile and flexural strength of GNs-filled PVDF nanocomposites all show significant improvement even at low graphene content. Such enhancement in thermal stability, tensile and flexural properties offers great promises for wider application of PVDF-based materials.

ACKNOWLEDGMENTS

This work was supported by Moroccan Foundation for Advanced Science, Innovation and Research (MAScIR), Rabat, Morocco. The authors thank Professor Abdelilah Benyoussef, Director of the Laboratory of Magnetism and High Energy Physics, Mohamed V University in Rabat for the fruitful discussion.

REFERENCES

1. Novoselov, K. S.; Geim, A. K.; Morozov, S. V.; Jiang, D.; Zhang, Y.; Dubonos, S. V.; Grigorieva, I. V.; Firsov, A. A. *Science* **2004,** *306*, 666.

2. Novoselov, K. S.; Jiang, Z.; Zhang, Y.; Morozov, S. V.; Stormer, H. L.; Zeitler, U.; Maan, J. C.; Boebinger, G. S.; Kim, P.; Geim, A. K. *Science* **2007,** *315*, 1379.

3. Lee, C.; Wei, X.; Kysar, J. W.; Hone, J. *Science* **2008,** *321*, 385.
4. Balandin, A. A.; Ghosh, S.; Bao, W.; Calizo, I.; Teweldebrhan, D.; Miao, F.; Lau, C. N. *Nano Lett.* **2008,** *8*, 902.
5. Stoller, M. D.; Park, S.; Zhu, Y.; An, J.; Ruoff, R. S. *Nano Lett.* **2008,** *8*, 3498.
6. Bolotin, K. I.; Sikes, K. J.; Jiang, Z.; Klima, M.; Fudenberg, G.; Hone, J.; Kim, P.; Stormer, H. L. *Solid State Commun.* **2008,** *146*, 351.
7. Wu, Z. S.; Ren, W.; Gao, L.; Zhao, J.; Chen, Z.; Liu, B.; Tang, D.; Yu, B.; Jiang, C.; Cheng, H. M. *ACS Nano* **2009,** *3*, 411.
8. Liu, N.; Luo, F.; Wu, H.; Liu, Y.; Zhang, C.; Chen, J. *Adv. Funct. Mater.* **2008,** *18*, 1518.
9. Behabtu, N.; Lomeda, J. R.; Green, M. J.; Higginbotham, A. L.; Kosynkin, D. V.; Tsentalovich, D.; Parra-Vasquez, A. N. G.; Schmidt, J.; Kesselman, E.; Cohen, Y.; Talmon, Y.; Tour, J. M.; Matteo, P. *Nat. Nanotechnol.* **2010,** *5*, 406.
10. Schniepp, H. C.; Li, J. L.; McAllister, M. J.; Sai, H.; Alonso, M. H.; Adamson, D. H.; Prud'homme, R. K.; Car, R.; Saville, D. A.; Aksay, I. A. *J. Phys. Chem. B* **2006,** *110*, 8535.
11. Wang, H.; Robinson, J. T.; Li, X.; Dai, H. J. *Am. Chem. Soc.* **2009,** *131*, 9910.
12. Williams, G.; Seger, B.; Kamat, P. V. *ACS Nano* **2008,** *2*, 1487.
13. Stankovich, S.; Dikin, D. A.; Piner, R. D.; Kohlhaas, K. A.; Kleinhammes, A.; Jia, Y.; Wu, Y.; Nguyen, S. T.; Ruoff, R. S. *Carbon* **2007,** *45*, 1558.
14. Wang, G.; Yang, J.; Park, J.; Gou, X.; Wang, B.; Liu, H.; Yao, J. J. *Phys. Chem. C* **2008,** *112*, 8192.
15. Gao, W.; Alemany, L. B.; Ci, L.; Ajayan, P. M. *Nat. Chem.* **2009,** *1*, 1403.
16. Chen, W.; Yan, L.; Bangal, P. R. *J. Phys. Chem. C* **2010,** *114*, 19885.
17. Fan, Z. J.; Kai, W.; Yan, J.; Wei, T.; Zhi, L. J.; Feng, J.; Ren, Y.; Song, L. P.; Wei, F. *ACS Nano* **2011,** *5*, 191.
18. Stankovich, S.; Dikin, D. A.; Dommett, G. H. B.; Kohlhaas, K. M.; Zimney, E. J.; Stach, E. A.; Piner, R. D.; Nguyen, S. T.; Ruoff, R. S. *Nature* **2006,** *442*, 282.
19. Zhao, X.; Zhang, Q.; Chen, D.; Lu, P. *Macromolecules* **2010,** *43*, 2357.
20. Ramanathan, T.; Abdala, A. A.; Stankovich, S.; Dikin, D. A.; Herrera-Alonso, M.; Piner, R. D.; Adamson, D. H.; Schniepp, H. C.; Chen, X.; Ruoff, R. S.; Nguyen, S. T.; Aksay, I. A.; Prud'Homme, R. K.; Brinson, L. C. *Nat. Nanotechnol.* **2008,** *3*, 327.
21. Xu, Z.; Gao, C. *Macromolecules* **2010,** *43*, 6716.
22. Hu, H.; Wang, X.; Wang, J.; Wan, L.; Liu, F.; Zheng, H.; Chen, R.; Xu, C. *Chem. Phys. Lett.* **2010,** *484*, 247.
23. Kim, H.; Miura, Y.; Macosko, C. W. *Chem. Mater.* **2010,** *22*, 3441.
24. Kim, H.; Kobayashi, S.; AbdurRahim, M. A.; Zhang, M. J.; Khusainova, A.; Hillmyer, M. A.; Abdala, A. A.; Macosko, C. W. *Polymer* **2011,** *52*, 1837.
25. Zhang, H. B.; Zheng, W. G.; Yan, Q.; Yang, Y.; Wang, J. W.; Lu, Z. H.; Ji, G. Y.; Yu, Z. Z. *Polymer* **2010,** *51*, 1191.
26. Kim, H.; Macosko, C. W. *Macromolecules* **2008,** *41*, 3317.
27. Kim, H.; Macosko, C. W. *Polymer* **2009,** *503*, 3797.
28. Steurer, P.; Wissert, R.; Thomann, R.; Mülhaupt, R. *Macromol. Rapid Commun.* **2009,** *30*, 316.
29. Ansari, S.; Giannelis, E. P. *J. Polym. Sci. Part B: Polym. Phys.* **2009,** *47*, 888.
30. Layek, R. K.; Samanta, S.; Chatterjee, D. P.; Nandi, A. K. *Polymer* **2010,** *51*, 5846.
31. El Achaby, M.; Arrakhiz, F. Z.; Vaudreuil, S.; Essassi, E. M.; Qaiss, A. *Appl. Surf. Sci.* **2012,** *258*, 7668.
32. El Achaby, M.; Arrakhiz, F. Z.; Vaudreuil, S.; Qaiss, A.; Bousmina, M.; Fassi-Fehri, O. *Polym. Compos.* **2012,** *33*, 733.
33. Hummers, W. S.; Offeman, R. E. *J. Am. Chem. Soc.* **1958,** *80*, 1339.
34. Li, D.; Müller, M. B.; Gilje, S.; Kaner, R. B.; Wallace, G. G. *Nat. Nanotechnol.* **2008,** *3*, 10.
35. Acik, M.; Mattevi, C.; Gong, C.; Lee, G.; Cho, K.; Chhowalla, M.; Chabal, Y. J. *ACS Nano* **2010,** *4*, 5861.
36. Ju, H. M.; Huh, S. H.; Choi, S. H.; Lee, H. L. *Mater. Lett.* **2010,** *64*, 357.
37. Zhu, P.; Shen, M.; Xiao, S.; Zhang, D. *Physica B* **2011,** *406*, 498.
38. Fernandez-Merino, M. J.; Guardia, L.; Paredes, J. I.; Villar-Rodil, S.; Solis-Fernandez, P.; Martınez-Alonso, A.; Tascon, J. M. D. *J. Phys. Chem. C* **2010,** *114*, 6426.
39. Coleman, J. N.; Cadek, M.; Blake, R.; Nicolosi, V.; Ryan, K. P.; Belton, C.; Fonseca, A.; Nagy, J. B.; Gun'ko, Y. K.; Blau, W. J. *Adv. Funct. Mater.* **2004,** *14*, 791.
40. Buckley, J.; Cebe, P.; Cherdack, D.; Crawford, J.; Ince, B. S.; Jenkins, M.; Pan, J.; Reveley, M.; Washington, N.; Wolchover, N. *Polymer* **2006,** *47*, 2411.
41. Patole, A. S.; Patole, S. P.; Kang, H.; Yoo, J. B.; Kim, T. H.; Ahn, J. H. *J. Colloid Interf. Sci.* **2010,** *350*, 530.
42. Zanetti, M.; Camino, G.; Reichert, P.; Mulhaupt, R. *Macromol. Rapid Commun.* **2001,** *22*, 176.
43. Yang, J.; Lin, Y.; Wang, J.; Lai, M.; Li, J.; Liu, J.; Tong, X.; Cheng, H. J. *Appl. Polym. Sci.* **2005,** *98*, 1087.
44. Chatterjee, A.; Deopura, B. L. *J. Appl. Polym. Sci.* **2006,** *100*, 3574.
45. Patro, T. U.; Mhalgi, M. V.; Khakhar, D. V.; Misra, A. *Polymer* **2008,** *49*, 3486.
46. Peng, Q. Y.; Cong, P. H.; Liu, X. J.; Liu, T. X.; Huang, S.; Li, T. S. *Wear* **2009,** *266*, 713.